BIOCHEMISTRY
including biophysical chemistry & molecular biology

Article

pubs.acs.org/biochemistry

Isolation and Structural and Pharmacological Characterization of α-Elapitoxin-Dpp2d, an Amidated Three Finger Toxin from Black Mamba Venom

Ching-I Anderson Wang,[§] Timothy Reeks,[§] Irina Vetter, Irene Vergara, Oleksiy Kovtun, Richard J. Lewis, Paul F. Alewood, and Thomas Durek*

Division of Chemistry and Structural Biology, Institute for Molecular Bioscience, The University of Queensland, St Lucia, Brisbane, Queensland 4072, Australia

ABSTRACT: We isolated a novel, atypical long-chain three-finger toxin (TFT), α-elapitoxin-Dpp2d (α-EPTX-Dpp2d), from black mamba (*Dendroaspis polylepis polylepis*) venom. Proteolytic digestion with trypsin and V8 protease, together with MS/MS *de novo* sequencing, indicated that the mature toxin has an amidated C-terminal arginine, a posttranslational modification rarely observed for snake TFTs. α-EPTX-Dpp2d was found to potently inhibit α7 neuronal nicotinic acetylcholine receptors (nAChR; IC_{50}, 58 ± 24 nM) and muscle-type nAChR (IC_{50}, 114 ± 37 nM) but did not affect α3β2 and α3β4 nAChR isoforms at 1 μM concentrations. Competitive radioligand binding assays demonstrated that α-EPTX-Dpp2d competes with epibatidine binding to the *Lymnea stagnalis* acetylcholine-binding protein (*Ls*-AChBP; IC_{50}, 4.9 ± 2.3 nM). The activity profile and binding data are reminiscent of classical long-chain TFTs with a free carboxyl termini, suggesting that amidation does not significantly affect toxin selectivity. The crystal structure of α-EPTX-Dpp2d was determined at 1.7 Å resolution and displayed a dimeric toxin assembly with each monomer positioned in an antiparallel orientation. The dimeric structure is stabilized by extensive intermolecular hydrogen bonds and electrostatic interactions, which raised the possibility that the toxin may exist as a noncovalent homodimer in solution. However, chemical cross-linking and size-exclusion chromatography coupled with multiangle laser light scattering (MALLS) data indicated that the toxin is predominantly monomeric under physiological conditions. Because of its high potency and selectivity, we expect this toxin to be a valuable pharmacological tool for studying the structure and function of nAChRs.

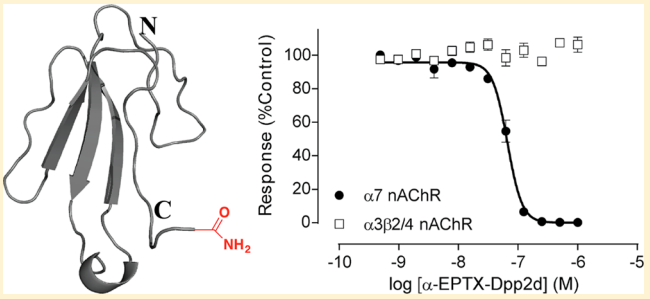

Three-finger toxins (TFTs) form one of the largest families of bioactive molecules found in the venom of snakes, particularly those from the Elapidae family.[1] They are polypeptides of about 60−75 amino acids, which form a compact core structure stabilized by four conserved disulfide bridges from which three loops (fingers) protrude.[2] A number of TFTs contain a fifth disulfide bond in either loop I (nonconventional TFTs) or loop II (long chain TFTs).[2] Snake TFTs are structurally and functionally heterogeneous. Sequence variation in the loops facilitates functional adaptability and allows TFTs to recognize a broad range of molecular targets with exquisite specificity.[2] According to their mode of action, they can be classified as neurotoxins (targeting either acetylcholine esterase, L-type calcium channels, or nicotinic or muscarinic acetylcholine receptors), cardiotoxins, or platelet aggregation inhibitors. The molecular diversity of TFTs is the result of gene duplication of key regulatory household proteins that can result in many isoforms from the same protein molecular scaffold.[3] Most toxins act as monomers and exhibit biological activity against essential physiological systems with a variable degree of potency.[2] However, other components of the venom often act synergistically to enhance the overall potency of the venom.[4] Complexes can be formed between toxins through either covalent[5,6] or noncovalent[7,8] interactions. Subtle perturbations to the bioactive pharmacophore due to conformational changes induced by complex formation generally lead to an increase in toxicity from either the larger or novel binding surface.[4] Such complexes may be as intricate as the heterohexameric PLA_2 textilotoxin from *Pseudonaja textilis*[9] or as modest as the covalently linked heterodimeric TFT irditoxin from the colubrid *Boiga irregularis*.[6]

Because of their high specificity, selectivity, and potency, these toxins have proven invaluable as pharmacological tools for studying the structure, function, and distribution of their respective target receptors.[1] Nevertheless, the majority of the more than 500 TFT sequences that have been determined so far remain poorly characterized on a structural and functional level. In fact for a significant fraction, a molecular target has yet to be identified (orphan TFTs). Clearly, despite more than 50 years of research into TFTs, much remains to be discovered for this exciting class of molecules.

Received: April 11, 2014
Revised: May 26, 2014
Published: May 27, 2014

   dx.doi.org/10.1021/bi5004475 | *Biochemistry* 2014, 53, 3758−3766

In our efforts to characterize individual components from the venom of black mamba (*Dendroaspis polylepis polylepis*) we identified a novel TFT with uncharacteristic structural features. The new toxin (α-elapitoxin-Dpp2d) features an amidated C-terminus, a posttranslational modification uncommon for TFTs. We here report the isolation, X-ray structure and pharmacological characterization of α-elapitoxin-Dpp2d.

EXPERIMENTAL PROCEDURES

Toxin Purification. α-Elapitoxin-Dpp2d (α-EPTX-Dpp2d) was purified from crude *Dendroaspis polylepis polylepis* (black mamba) venom. Venom was purchased from Latoxan (France) and contained pooled samples from South African black mambas. The crude lyophilized venom (30 mg) was dissolved in 1.5 mL of buffer A (10 mM KH_2PO_4, 20% (v/v) acetonitrile, pH 2.6) at a concentration of 20 mg/mL. The solution was filtered through 0.22 μm filter cartridges and loaded onto a HPLC cation-exchange column (polysulfethyl A, 10 × 100 mm^2, 5 μm particle size, 300 Å pore size) equilibrated with buffer A. Venom components were eluted using a linear gradient of 0−10% buffer B (10 mM KH_2PO_4, 1 M KCl, 20% (v/v) acetonitrile, pH 2.6) in buffer A over 5 min at a flow rate of 5 mL/min, followed by a linear gradient of 10−100% buffer B in buffer A over 55 min. Fractions were collected across the entire elution range based on eluent absorption at 214 and 280 nm. Fractions containing α-EPTX-Dpp2d as determined by mass spectrometry (MS) were pooled, and acetonitrile was removed under vacuum in a SpeedVac. The concentrated sample (~5 mL) was loaded onto a Vydac C18 reversed-phase column (10 × 250 mm^2) equilibrated with 10% buffer D (90% acetonitrile, 0.043% TFA in water) in buffer C (0.05% TFA in water). Peptides were eluted using a linear gradient of 10−45% buffer D in buffer C over 50 min. Fractions containing α-EPTX-Dpp2d were pooled and lyophilized. The processing of 180 mg of crude venom yielded 1.5 mg of pure toxin (~0.8% isolated yield). High-resolution ESI-MS on a triple TOF 5600 system (ABSCIEX) was used to determine the molecular weight (MW) of the toxin (monoisotopic mass 7985.33 ± 0.40 Da).

***De Novo* Peptide Sequencing.** Lyophilized, purified toxin (20 μg) was dissolved in water (45 μL), and 5 μL of 25 mM ammonium carbonate (pH 7.8) was added. Reduction/alkylation was performed by adding 50 μL of a 97.5% acetonitrile, 2% iodoethanol, and 0.5% triethylphosphine (v/v/v) cocktail. Samples were incubated for 120 min at 37 °C and subsequently dried in a SpeedVac. The peptide was reconstituted in 100 mM ammonium carbonate (pH 8.5) and trypsin (1.0 mg/mL in 1.0 mM HCl) added to give a protease to peptide ratio of 1:20. For endoproteinase Glu-C digestion, the peptide was reconstituted in 25 mM ammonium carbonate (pH 7.8), and enzyme (1.0 mg/mL MQ water) was added to a protease to peptide ratio of 1:20. Both samples were incubated overnight at 37 °C.

Samples were freeze-dried and reconstituted in 0.1% formic acid solution. The extracts were analyzed by LC-MSMS on a Shimadzu Nexera uHPLC (Japan) coupled to a Triple TOF 5600 mass spectrometer (ABSCIEX, Canada) equipped with a duo electrospray ion source. Aliquots (2 μL) of extracts were injected onto a 2.1 mm × 100 mm Zorbax SB 300 Å C18 1.8 μm column (Agilent) at 250 μL/min. Solvent A consisted of 0.1% (v/v) formic acid in water, and solvent B contained 90% (v/v) acetonitrile and 0.1% (v/v) formic acid in water. Linear gradients of 1−40% solvent B over 25 min at 250 μL/min flow rate were used for protein elution. The ion-spray voltage was set to 5300 V, declustering potential at 100 V, curtain gas flow at 25 psi, nebulizer gas flow at 45 psi, heater gas flow to 35 psi, interface heater at 150 °C, and the turbo heater to 450 °C. The mass spectrometer acquired 250 ms full scan TOF-MS data followed by 20 50 ms full scan product ion acquisitions in an information dependent acquisition (IDA) mode. Full scan TOF-MS data was acquired over the mass range 300−2000 Da and for product ion ms/ms 80−2000 Da. Ions observed in the TOF-MS scan exceeding a threshold of 150 counts and a charge state of +2 to +5 were set to trigger the acquisition of product ion MSMS spectra of the resultant 20 most intense ions. The data was acquired and processed using Analyst TF 1.5.1 software (AB SCIEX, Canada). Interpretation of spectral data for *de novo* sequencing was performed manually, aided by both Analyst TF 1.5.1 and Protein Pilot v4 software (AB SCIEX, Canada).

Crystallization and Structure Determination. Crystals of the venom-purified α-EPTX-Dpp2d were obtained by the hanging drop vapor diffusion technique at 20 °C. Lyophilized toxin was dissolved in 2 mM HCl at a concentration of 5 mg/mL. The hanging drop consisted of 1 μL of protein solution mixed with 1 μL of reservoir solution (0.1 M TRIS-HCL, pH 7.5, 2% (v/v) dioxane, 65% (v/v) 2-methyl-2,4-pentanediol (MPD)) and was equilibrated against 500 μL of reservoir solution. Cubic and rod-shaped crystals appeared after 5−7 days and grew to dimensions of about 0.5 × 0.5 × 0.25 mm^3. The X-ray diffraction data sets were collected in a cryostream (100 K) with a Rigaku Saturn 944 CCD detector and Cu Kα radiation from a Rigaku FR-E+ SuperBright generator (Rigaku/MSC) at the University of Queensland, Australia. The raw data sets were autoindexed, integrated, and scaled using the CrystalClear 2.0 package (Rigaku/MSC) and iMOSFLM.[10] The structure was determined by molecular replacement with the program Phaser,[11] using the crystal structure of neurotoxin-1 from *Naja naja oxiana* venom (PDB ID 1NTN)[12] as a search model. An excellent quality of the electron density map was obtained at this stage, which allowed ~80% of the model to be autobuilt using Arp/Warp.[13] The resulting model with the electron density map was examined to manually build the rest of the model using Coot.[14] The map fitting and structure refinement was performed using Coot and REFMAC5,[15] respectively, until satisfactory model statistics were obtained (Table 1). The structure quality analysis was done using web server Molprobity[16] and SFcheck[17] in the CCP4i program suite.[18] Structural coordinates for α-EPTX-Dpp2d have been deposited in the protein data bank (PDB ID 4LFT).

Docking Simulations. Monomeric (subunit B) and dimeric α-EPTX-Dpp2d (PDB ID 4LFT) were docked to *Ls*-AChBP extracted from the cocrystal structure of α-cobratoxin/*Ls*-AChBP (PDB ID 1YI5)[19] using Haddock.[20] Residues in the middle finger (D28−K36) of α-EPTX-Dpp2d were selected to be active residues for docking as observed for α-cobratoxin. The passive residues, which are solvent exposed and surround the active residues, were defined automatically by Haddock. Semiflexible and fully flexible regions were automatically detected by Haddock, and sampling parameters were set as default. Sampling and cluster parameters were default values, except that 2000 structures were calculated for rigid body docking, with the best 400 solutions then subjected to semiflexible simulated annealing and explicit solvent refinement. The Haddock score, minimal energy, existing experimental data, and multiplicity of the same docking orientation

dx.doi.org/10.1021/bi5004475 | *Biochemistry* 2014, 53, 3758−3766

Table 1. Statistics for X-ray Data Collection and Structure Refinement

data collection	Rigaku Saturn944
space group	$P2_12_12_1$
cell dimensions	
a, *b*, *c* (Å)	104.60, 38.27, 39.42
α, β, γ (deg)	90.0, 90.0, 89.99
resolution (Å)	34.87−1.70 (1.74−1.70)
reflections	
observed	121 995
unique	22 047
redundancy	5.53 (2.16)
completeness (%)	92.85 (91.3)
R_{merge}	0.045 (0.483)
$I/\sigma(I)$	27.2 (1.9)
refinement	
resolution (Å)	27.46−1.70
R_{work}/R_{free}	0.23/0.28
no. atoms	
protein	1034
water	133
B-factor (Å^2)	
protein	23.9
water	33.8
rms deviations	
bond lengths (Å)	0.024
bond angles (deg)	2.267
Ramachandran plot	
most favored regions (%)	97.7
allowed regions (%)	2.3

(RMSD < 7.5 Å) were used as selection criteria for choosing possible binding modes. The cluster with the best (most negative) Haddock scores for α-EPTX-Dpp2d (−96.9 ± 4.9) are shown in Figure 5C.

Cross-Linking and Electrophoresis. Toxin at a concentration of 100 nM was used for the cross-linking experiment with bis[sulfosuccinimidyl] suberate (BS3) cross-linker and a peptide to cross-linker ratio of 1:20 in 200 μL of PBS solution (pH 7.4) as described in the manufacturer's instruction (Pierce). Cross-linking of the samples was terminated after 1 h by addition of Tris buffer to give a final concentration of 50 mM. The samples were analyzed by SDS-PAGE using 4−12% Nu-Page gels (Invitrogen) and silver staining (Invitrogen) to determine the oligomerization status under denaturing and reducing conditions.

Size Exclusion Chromatography-Multiangle Laser Light Scattering (SEC-MALLS). SEC-MALLS analysis was conducted as described previously using a miniDAWN Tristar laser light scattering photometer and an Optilab DSP interferometric refractometer (Wyatt Technology).[21] Venom-purified α-EPTX-Dpp2d in water (20 μL, 10 mg/mL) was injected onto a WTC-030S5 SEC column (7.8 × 300 mm^2, Wyatt Technology) and resolved in 20 mM HEPES-KOH, 150 mM NaCl buffer. Experimental profiles of refraction and light scattering data were used to determine peptide molecular weight using Debye solution of Zimm's model for light scattering[22] as implemented in the ASTRA software package (Wyatt Technology).[21] Instrument calibration was verified with a sample of bovine serum albumin.

Expression and Purification of *Ls*-AChBP in *Escherichia coli*. The expression and purification protocol of *Ls*-AChBP is similar to that previously described[23,24] with minor modifications. Briefly, the *Ls*-AChBP cDNA was codon-optimized for expression in *E. coli*, cloned into a pHUE expression vector, and expressed as a His_6-tagged ubiquitin fusion protein (Ub−*Ls*-AChBP). The Ub−*Ls*-AChBP expression was induced with IPTG (final concentration 1 mM) as OD_{600} reached ∼0.8, at 16 °C for 18 h. Cells were harvested by centrifugation at 6000*g* at 4 °C and lysed with three freeze−thaw cycles followed by brief (1 min) sonication. Cell debris were removed from the supernatant by centrifugation at 39000*g* at 4 °C. Ub−*Ls*-AChBP was first purified using Talon resin (Scientifix) followed by size exclusion chromatography using a Superdex 200 10/300 column (GE Healthcare). The purity was determined by SDS-PAGE, and the pentameric oligomerization state was verified by size exclusion chromatography. Competitive epibatidine radioligand-binding assays were used to confirm the functional integrity of the fusion protein (see below).

Radioligand-Binding Assay. The α-EPTX-Dpp2d binding affinity was determined by displacement of [^{3}H]epibatidine from Ub−*Ls*-AChBP. Displacement of [^{3}H]epibatidine by unlabeled epibatidine was used as positive control (IC_{50} 4.6 ± 2.1 nM, n = 4). The radioligand binding assay was performed in a 96-well plate format using the flexible plate format (PerkinElmer Life and Analytical Sciences). The coating with Ub−*Ls*-AChBP was achieved by aliquoting 100 μL of purified Ub−*Ls*-AChBP at a final concentration of 43 nM in PBS in each well followed by an overnight incubation at 4 °C. To reduce nonspecific radioligand adsorption, 150 μL of 0.05% BSA (Sigma-Aldrich, Australia) in PBS was added to each well, and plates were incubated on ice for 1 h. The assays were performed with a fixed concentration of [^{3}H]epibatidine of 1 nM and serial dilutions of venom-purified α-EPTX-Dpp2d or epibatidine ranging from 10^{-5} to 10^{-15} M in a final volume of 100 μL. Plates were incubated on ice for 1 h. The solutions were discarded, and wells were washed twice with 150 μL of 0.05% BSA. Optisafe Supermix scintillant (100 μL; PerkinElmer Life and Analytical Sciences) was added to each well, and the plates were sealed before analysis in a MicroBeta counter (PerkinElmer Life and Analytical Sciences). The nonspecific binding of [^{3}H]epibatidine was determined in the presence of 100 μM epibatidine, and the specific [^{3}H]epibatidine binding was calculated as the difference between the measured radioactivity and the nonspecific binding. The radioligand binding assays for α-EPTX-Dpp2d and epibatidine were performed in triplicate and repeated three times. IC_{50} values are reported as mean ± standard deviation of the mean (n = 4).

Functional Activity at Human α7 and $\alpha3\beta2/\alpha3\beta4$ nAChR. SH-SY5Y human neuroblastoma cells (European Collection of Cell Cultures) were routinely maintained in RPMI medium (Invitrogen, Australia) supplemented with 15% fetal bovine serum and L-glutamine and passaged every 3−5 days using 0.25% trypsin/EDTA (Invitrogen). To assess the activity of venom-purified α-EPTX-Dpp2d at human α7 and $\alpha3\beta2/\alpha3\beta4$ nAChR, inhibition of Ca^{2+} responses evoked by choline or nicotine were assessed using a FLIPR high-throughput assay as previously described.[25] In brief, human SH-SY5Y neuroblastoma cells were plated on black-walled 384-well imaging plates (Corning, density 35000−50000 cells/well) prior to loading with fluorescent Ca^{2+} dye (calcium 4 no wash dye, Molecular Devices) diluted in physiological salt solution (PSS, composition in mM: NaCl 140, glucose 11.5, KCl 5.9, $MgCl_2$ 1.4, NaH_2PO_4 1.2, $NaHCO_3$ 5, $CaCl_2$ 1.8, HEPES 10).

dx.doi.org/10.1021/bi5004475 | *Biochemistry* 2014, 53, 3758−3766

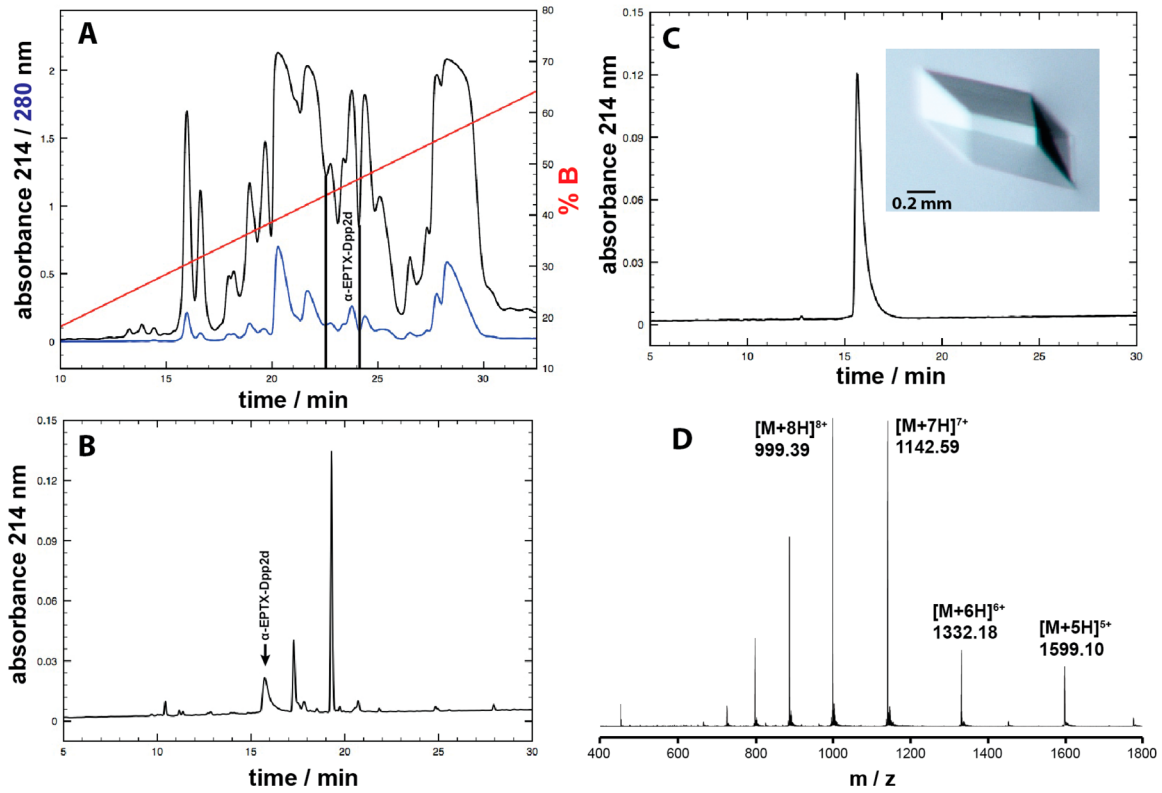

Figure 1. Purification of α-EPTX-Dpp2d. (A) Cation-exchange chromatogram of crude *Dendroaspis polylepis polylepis* venom. The indicated fraction contained the three finger long-chain neurotoxin α-EPTX-Dpp2d. (B) Reversed-phase HPLC chromatogram of fraction "α-EPTX-Dpp2d" obtained after IEX chromatography. (C) Purified α-EPTX-Dpp2d toxin after preparative RP-HPLC. (D) High-resolution ESI-MS spectrum of the isolated toxin. Data deconvolution indicated a mass of M_{found} = 7985.33 Da (M, most abundant isotope composition).

After 30 min incubation at 37 °C, fluorescence responses (excitation 470−495 nm; emission 515−575 nm) to stimulation with the agonists choline (α7) or nicotine (α3β2/α3β4) were assessed using the FLIPR^{Tetra} fluorescent plate reader (Molecular Devices) after 5 min pretreatment with α-EPTX-Dpp2d. Nicotine (30 μM) was used to activate endogenously expressed human α3β2 and α3β4 nAChR, while endogenously expressed human α7 nAChR was activated using the α7 nAChR agonist choline (30 μM) in the presence of the allosteric modulator PNU120596 (10 μM, Sigma-Aldrich). Raw fluorescence readings were converted to response over baseline using the analysis tool Screenworks 3.2.0.14 (Molecular Devices) and were expressed relative to the maximum increase in fluorescence of control responses. Concentration−response curves were plotted using GraphPad Prism (version 5.03, SanDiego, CA, USA) by fitting the data to a four-parameter Hill equation with variable slope. IC_{50} values are reported as mean ± standard error of the mean (n = 4 independent experiments with a minimum of three replicates per concentration).

Functional Activity at Human α1β1γδ nAChR. To assess activity at muscle-type nAChR, human TE-671 cells endogenously expressing α1β1γδ nAChR[26] were plated at a density of 30000 cells/well on 384-well plates and loaded with red membrane potential dye (Molecular Devices) for 30 min at 37 °C. Responses to stimulation with nicotine (100 μM) were assessed after 5 min pretreatment with varying concentrations of α-EPTX-Dpp2d and α-bungarotoxin using the FLIPR fluorescent plate reader (excitation 510−545 nm; emission 656−625 nm).

RESULTS

Toxin Isolation and Primary Structure. We isolated a novel peptide from crude black mamba venom using a combination of cation-exchange and reversed-phase HPLC under denaturing conditions (Figure 1A−C). The putative toxin was isolated in a highly pure form in 0.8% yield and had a monoisotopic MW of 7985.33 ± 0.40 Da as determined by high-resolution ESI-MS (Figure 1D). A search of the UNIPROT database revealed no matches to known *D. polylepis* sequences suggesting a previously uncharacterized molecule and, based on the observed MW, a likely new member of the TFT family. The molecule was reduced and alkylated with 2-iodoethanol, which was accompanied by a shift in MW (Δ = +449.92 Da) indicative of ten cysteine residues, which are likely to form five disulfide bonds in the native molecule (later confirmed by X-ray structure, see below). Proteolytic digestion of the reduced and alkylated peptide with endoproteinase Glu-C or trypsin in separate reactions resulted in six and ten peptide fragments, respectively, which where subjected to LC-MSMS *de novo* sequencing. Both data sets consisting of overlapping peptide segments were generally in good agreement with each other and were used to manually assemble the mature toxin sequence. However, a significant discrepancy between trypsin and Glu-C digested samples was observed for peptide segments corresponding to the C-terminus (Figure 2). Fragmentation of the Glu-C C-terminal peptide produced *y* ions consistent with an amidated C-terminus (Figure 2A), whereas the C-terminal peptide derived from tryptic digests produced *y* ions in agreement with a free carboxyl C-terminus (Figure 2B). The C-terminal residue was subsequently identified as Arg72

dx.doi.org/10.1021/bi5004475 | *Biochemistry* 2014, 53, 3758−3766

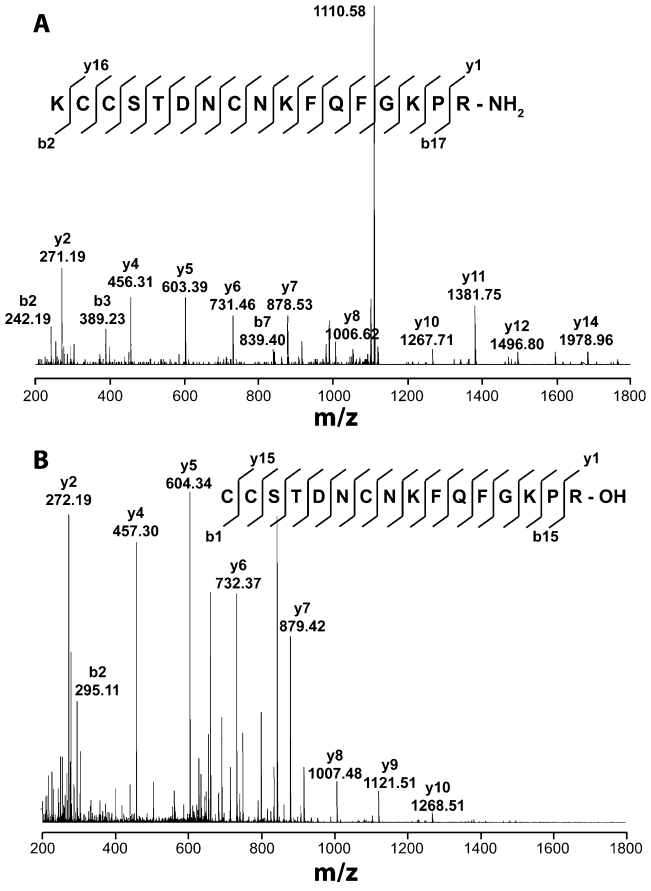

Figure 2. MS/MS spectra derived from C-terminal peptide fragments obtained after proteolytic digestion with Endo-GluC (A, parent ion, 2218.99 Da) or trypsin (B, parent ion, 1978.80 Da).

suggesting that trypsin catalyzed deamidation of the native molecule and release of ammonia. Identification of all isobaric residues (Leu/Ile) or near-isobaric residues (Gln/Lys) as well as any other ambiguity was resolved by interpreting the high-resolution (1.7 Å) electron density map (see below). The final primary structure is shown in Figure 3A. Its theoretical monoisotopic MW (taking into account C-terminal amidation and formation of five disulfide bridges) of 7985.76 Da is in excellent agreement with the experimentally determined value (7985.33 ± 0.40 Da).

A BLAST search of the derived sequence indicated high similarity to snake TFT nAChR antagonists and to previously identified long-chain neurotoxins from black mamba (α-EPTX-Dpp2a-c, Figure 3A).[27] Comparison to the three latter toxins revealed notable differences in the putative pharmacophore region (Phe/Trp in position 30) as well as the C-terminal region (Figure 3A). Following biochemical characterization, the new toxin was named α-elapitoxin-Dpp2d (α-EPTX-Dpp2d), and the sequence was deposited in UNIPROT.

Three-Dimensional Structure. Native α-EPTX-Dpp2d was crystallized and its structure solved by molecular replacement using the crystal structure of neurotoxin-1 from *Naja naja oxiana* (PDB ID 1NTN)[12] as a search model. The structure was carefully refined at 1.7 Å with a final R_{work} and R_{free} of 0.23 and 0.28, respectively (Table 1, Figure 3B). Each asymmetric unit consists of two α-EPTX-Dpp2d molecules (hereafter called subunit A and B) forming a noncovalent dimer via a network of van der Waals interactions, four main chain−main chain hydrogen bonds, two main chain−side chain hydrogen bonds, and two interlocked salt bridges (E54−K56), with a noncrystallographic 2-fold symmetry (Figure 3C). Superimposition of the two α-EPTX-Dpp2d subunits showed that both are highly similar to a rmsd of 0.385 Å over 360 atoms. Minor differences occur between residues 6−12 in finger I (rmsd of 3.4 Å) and 28−36 in finger II (rmsd of 3.4 Å),

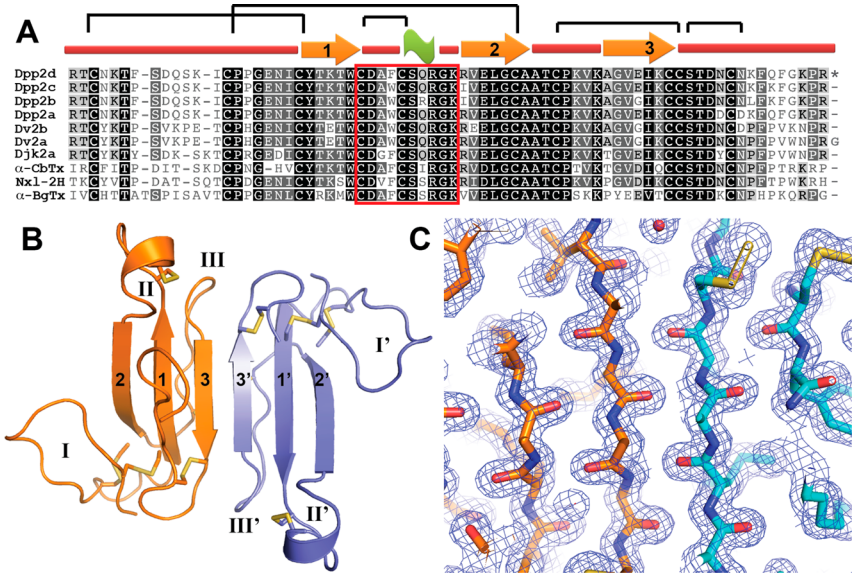

Figure 3. Overview of α-EPTX-Dpp2d structure (PDB ID 4LFT). (A) Primary sequence of α-EPTX-Dpp2d and alignment with closest long-chain TFT homologues from *Dendroaspis polylepis* (Dpp), *D. viridis* (Dv), *D. jamesoni kaimosae* (Djk) and other representative members from elapids (α-BgTx, α-CbTx, Nxl-2H). Observed secondary structure elements and the disulfide framework are shown at the top. The pharmacophores are highlighted with a red box. (B) Ribbon representation of the dimeric α-EPTX-Dpp2d structure. Fingers and β-strands are labeled with roman and arabic numerals, respectively. (C) $2F_o - F_c$ map of the α-EPTX-Dpp2d dimerization interface. The map was contoured at a level of 1.0 σ and is shown in the same orientation as in the structures in panel B.

dx.doi.org/10.1021/bi5004475 | *Biochemistry* 2014, 53, 3758−3766

which appear to originate from differences in the crystal packing interfaces. The flexible C-terminal tail (K65−R72) is only observed in subunit B presumably due to its tight crystal packing with three other asymmetry molecules, whereas the C-terminal tail of subunit A is not involved in crystal packing at all. Each α-EPTX-Dpp2d subunit consists of the four invariant disulfide bonds (C3−C21, C14−C42, C46−C57, C58−C63), which stabilize the TFT core. A fifth disulfide bond (C27−C31) is located at the tip of the long middle finger, similar to previously determined structures of long chain neurotoxins (Figure 3). Three antiparallel β-strands (1, 2, and 3) form a central three-stranded β-sheet in each subunit, which then extends to form a concave-shaped six-stranded antiparallel β-sheet with the other subunit. Both α-EPTX-Dpp2d monomers lack the two conserved N-terminal antiparallel β-strands in finger I found in most other TFTs. Structural analysis of α-EPTX-Dpp2d confirmed it as a novel long-chain TFT with high similarity to neurotoxins targeting nAChR.

Pharmacology. To assess biological activity, we resorted to a previously established high-throughput fluorescence assay.[25,28] SH-SY5Y neuroblastoma cells endogenously express human neuronal homopentameric α7, as well as heteropentameric α3β2 and α3β4 nAChRs.[25] Nicotine (30 μM) was used to activate endogenously expressed human α3β2 and α3β4 nAChR, while endogenously expressed human α7 nAChR was activated using the α7 nAChR agonist choline (30 μM) in the presence of the allosteric modulator PNU120596 (10 μM).[25] This caused a transient increase in intracellular Ca^{2+}, which was monitored on a FLIPR^{TETRA} by using a calcium-sensitive fluorescent dye. Treatment of cells with increasing concentrations of α-EPTX-Dpp2d led to a concentration-dependent block of choline-evoked Ca^{2+} responses, indicative of α7 antagonistic activity with an IC_{50} of 58 ± 24 nM (n = 4; Figure 4A). Nicotine-evoked responses were not affected by up to 1.0 μM α-EPTX-Dpp2d suggesting that this toxin does not affect α3β2 or α3β4 nAChR isoforms. α-EPTX-Dpp2d also inhibited muscle-type nAChR endogenously expressed in the TE-671 cell line[26] with similar potency (IC_{50} 114 ± 37 nM) to α-bungarotoxin (IC_{50} 164 ± 41 nM; Figure 4B).

Binding of α-EPTX-Dpp2d to *Ls*-AChBP was measured by the displacement of [^{3}H]epibatidine (K_D = 2.5 ± 0.2 nM), a potent nAChR agonist that also targets the acetylcholine-binding site of *Ls*-AChBP.[29] Under these conditions, α-EPTX-Dpp2d acted as a competitive epibatidine antagonist with an IC_{50} of 4.9 ± 2.3 nM (Figure 4C), suggesting that the binding sites for both molecules substantially overlap.

Oligomerization of α-EPTX-Dpp2d. The antiparallel orientation of the α-EPTX-Dpp2d monomers observed in the dimer crystal structure is reminiscent of other noncovalent dimers of TFTs, particularly κ-bungarotoxin and haditoxin, which have been shown to exist as stable dimers in solution under physiological conditions.[7,30] To better define the nature of α-EPTX-Dpp2d dimerization, chemical cross-linking experiments at physiologically relevant concentrations (10 and 100 nM) were conducted, and oligomerization was analyzed via reducing and denaturing SDS-PAGE (Figure 5A). Under these conditions, we observed monomers and several oligomers (dimers, trimers, and tetramers) of α-EPTX-Dpp2d with the monomer and dimer being the dominant species.

To further confirm α-EPTX-Dpp2d oligomer formation in solution, we performed size-exclusion chromatography (SEC) coupled with multiangle laser light scattering (MALLS) detection. To prevent nonspecific interactions of the toxin with the stationary phase, we included 150 mM NaCl in the running buffer. Under these conditions, α-EPTX-Dpp2d eluted as a symmetric peak with an apparent MW of 8760 ± 160 Da indicative of a predominantly monomeric toxin (Figure 5B).

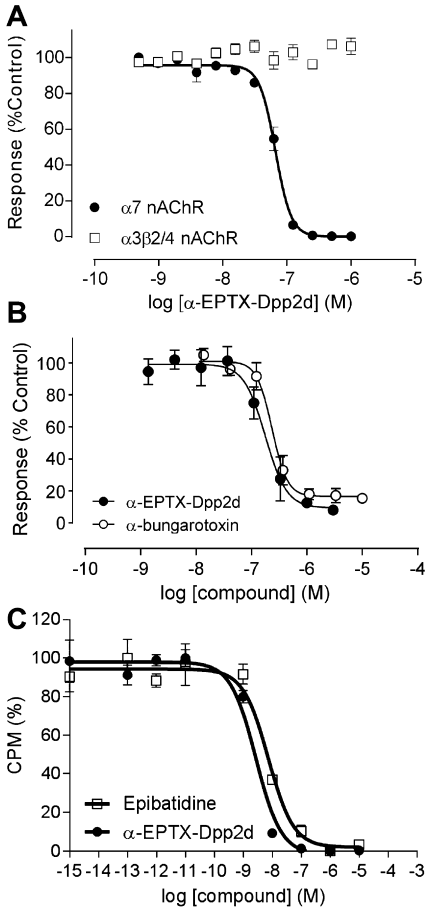

Figure 4. α-EPTX-Dpp2d is a potent inhibitor of human nAChRs. (A) Toxin concentration−response curves for α7 and α3β2/ α3β4 nAChRs endogenously expressed in SH-SY5Y cells (IC_{50} 58 ± 24 nM for α7 nAChR, n = 4). (B) Concentration−response curves for α-EPTX-Dpp2d (IC_{50} 114 ± 37 nM) and α-bungarotoxin (IC_{50} 164 ± 41 nM) on muscle-type nAChR. (C) α-EPTX-Dpp2d displaces [^{3}H]epibatidine (1 nM) from Ub−*Ls*-AChBP with an IC_{50} of 4.9 ± 2.3 nM (n = 4).

DISCUSSION

α-EPTX-Dpp2d was isolated as a minor component from black mamba venom using two chromatographic separation steps under denaturing (but disulfide-preserving) conditions. Ion-exchange chromatography was carried out first, because the high peptide-binding capacity of the chosen stationary phase allowed us to rapidly process large quantities (~180 mg) of crude venom with excellent resolution (Figure 1A). A second reversed-phase separation efficiently removed salts and gave pure toxin in an overall yield of 0.8% (Figure 1B,C). α-EPTX-Dpp2d is composed of 72 amino acids and five structure-stabilizing disulfide bonds in an arrangement highly similar to previously identified curaremimetic long-chain neurotoxins. The anticipated inhibitory activity of α-EPTX-Dpp2d at nAChR was confirmed at the homopentameric α7 nAChR (IC_{50} 58 ± 24 nM) and by competitive binding experiments with *Lymnea stagnalis* AChBP (IC_{50} 4.9 ± 2.3 nM). This activity profile is reminiscent of classical long-chain TFTs, such

dx.doi.org/10.1021/bi5004475 | *Biochemistry* 2014, 53, 3758−3766

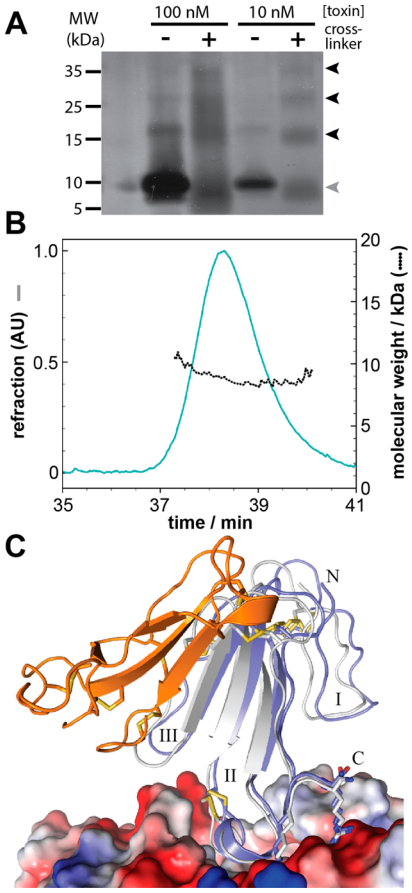

Figure 5. Analysis of α-EPTX-Dpp2d oligomerization. (A) SDS-PAGE analysis of non-cross-linked and cross-linked α-EPTX-Dpp2d at 10 and 100 nM concentrations. (B) SEC-MALLS analysis of α-EPTX-Dpp2d (at about 1 mM) indicates a MW of 8760 ± 160 Da suggesting that the toxin is primarily a monomer in solution. (C) Docking simulation of monomeric (white) and dimeric α-EPTX-Dpp2d (subunit A orange; subunit B cyan) at *Ls*-AChBP showed no difference in the binding mode, indicating that the dimer is capable of acting as a functional unit.

as α-bungarotoxin (α-BgTx) and α-cobratoxin (α-CbTx), which share high sequence similarity with α-EPTX-Dpp2d, particularly in the pharmacophore region (Figure 3A).[31] In contrast, α-EPTX-Dpp2d at concentrations up to 1 μM did not affect $\alpha3\beta2$ or $\alpha3\beta4$ nAChR isoforms, which are potently targeted by related κ-neurotoxins.[32]

During our MSMS *de novo* peptide sequencing attempts, we observed a consistent discrepancy of 1 Da when comparing the *y*-ions originating from the C-terminal peptide fragments derived from Glu-C and trypsin proteolytic digests (Figure 2). Because the C-terminal residue was subsequently identified as Arg72 and the ability of trypsin to hydrolyze Lys/Arg-carboxamides is well established,[33] we conclude that α-EPTX-Dpp2d is a novel C-terminally amidated snake TFT. Carboxamidation is a common posttranslational modification in cone snail, spider, and scorpion toxins but is uncommon for TFTs and rarely encountered in other snake toxins. C-terminal amidation is achieved *in vivo* by processing of a C-terminally elongated peptide precursor in a series of complex enzyme-catalyzed reactions.[34] Maeda and Tamiya were the first to report the sequence of two α-carboxamidated long-chain neurotoxins from *Astrotia stokesii*.[35] More recently, venom proteomic studies have sporadically provided further evidence of posttranslational C-terminal processing and amidation of snake TFTs, but none of these examples have been structurally and functionally characterized.[36] Indeed recent venom transcriptomic studies identified C-terminally elongated TFT mRNA transcripts that could not be fully correlated to translated proteins suggesting that the number of C-terminally processed snake TFTs might be substantially higher than previously thought.[37] C-terminal amidation is often required for full biological activity of mammalian peptide hormones such as calcitonin, oxytocin, and gastrin, but its functional and structural consequences on venom-derived peptide toxins are less well studied.[34] In the case of TFTs, structural and functional data indicate that the Arg/Lys-rich C-terminal tail contributes significantly to nAChR binding suggesting that C-terminal amidation may affect receptor recognition.[38−40] Trypsin is typically the protease of choice in proteomic studies because the generated peptide fragments have favorable ionization characteristics and upon fragmentation give rise to pronounced *y*-ion series. Our data indicate that care should be exercised with trypsin in venom proteomic studies when C-terminal lysine or arginine residues are encountered.

α-EPTX-Dpp2d adopts a TFT fold that resembles other known TFTs targeting nAChRs (Figure 3B). The similarity is particularly pronounced in the pharmacophore region located at the tip of finger II, which adopts a disulfide-stabilized α-helical turn conformation.

Based on the recently determined α-CbTx/AChBP complex structure, this motif inserts into a crevice at the interface between nAChR subunits.[19] Interestingly, the α-helical turn observed in finger II of α-EPTX-Dpp2d and other long chain α-neurotoxins is reminiscent of α-conotoxins (α-CTXs), which bind at the same site.[41] Despite the differences in disulfide connectivity and overall molecular size, the pharmacophores of both classes of molecules have a remarkably similar structural fold and share invariant residues important for inhibitory activity at $\alpha7$ nAChR and binding to AChBP. For example, aromatic and basic residues of α-CTX ImI (Arg7, Trp10) are also observed in reverse order in α-EPTX-Dpp2d (Phe30, Arg34).[42]

Covalent[5,6] or noncovalent[7,8] association of snake TFTs has recently been proposed as a strategy to create toxins with new activities not present in the individual monomers to further diversify the snake venom arsenal.[4] The dimerization interface of α-EPTX-Dpp2d shows striking similarity to haditoxin[7] (a homodimeric short-chain neurotoxin) and κ-bungarotoxin[30] (a homodimeric TFT targeting neuronal nAChR). In all structures, monomers associate in antiparallel orientation primarily by establishing a network of hydrogen bonds involving β-strands 3/3′ located in finger III resulting in formation of an extended six-pleated β-sheet. In light of these observations, it was of interest to examine whether the observed crystallographic α-EPTX-Dpp2d dimer structure is relevant in solution at physiological conditions and concentrations. Chemical cross-linking experiments using the bifunctional reagent BS3 indeed confirm dimer formation at low nanomolar toxin concentrations. However, concomitant formation of higher-order oligomers (trimers and tetramers) suggested that unspecific interactions may also be involved at least in part, which prompted us to explore alternative techniques. SEC-MALLS was used to determine the MW of α-EPTX-Dpp2d in solution.[21] The results indicate an apparent MW of ~8.7 kDa, suggesting that the toxin is predominately in the monomeric form under these conditions. The MW determined by SEC-

dx.doi.org/10.1021/bi5004475 | *Biochemistry* 2014, 53, 3758−3766

MALLS is approximately 9% higher than the value determined by ESI-MS (~8 kDa). This error is significantly above average for SEC-MALLS (<5%)[21] and may indicate a dynamic dimerization equilibrium. This is further supported by inspection of the molar mass distribution plot (Figure 5B), which indicates that the symmetric peak is not homogeneous with respect to MW tending to higher molecular weights toward the leading edge of the peak. Taken together these results are in agreement with α-EPTX-Dpp2d being mostly monomeric in solution and that dimerization is disfavored presumably because of a relatively fast dissociation rate.

To better understand the potential role of dimerization in receptor binding, we performed docking simulations of both monomeric (subunit B) and dimeric α-EPTX-Dpp2d to *Ls*-AChBP extracted from the cocrystal structure of α-CbTx/*Ls*-AChBP (PDB ID 1YI5).[19] Our simulations reveal that monomeric and dimeric toxin bind to *Ls*-AChBP in an almost identical mode suggesting that dimerization does not interfere with the finger II interactions with the ligand-binding site of AChBP (Figure 5C). It is noteworthy that subunit B is shown to bind at *Ls*-AChBP more preferably than subunit A in the dimer docking simulation. This is likely due to the presence of the positively charged C-terminal tail in subunit B (but not in subunit A) that appears to form additional electrostatic interactions with an acidic patch on AChBP (Figure 5C). Although these electrostatic interactions were not identified in the cocrystal structure of α-CbTx/*Ls*-AChBP due to the technical challenges and the nature of crystallization, it is likely that they are also present in the complex, as α-cobratoxin also contains an equivalent positively charged C-terminal tail.

In conclusion, we report the isolation and structural and pharmacological characterization of a novel C-terminally amidated long-chain α-neurotoxin (α-EPTX-Dpp2d) from crude *Dendroaspis polylepis polylepis* venom. Although the pharmacological consequences of C-terminal processing and amidation of TFTs are yet to be determined, it appears likely that this posttranslational modification (besides glycosylation[43] and oligomerization) represents another strategy for diversifying the toxin repertoire of venomous snakes. Our structural and pharmacological analysis reveals that α-EPTX-Dpp2d selectively inhibits α7 nAChRs and binds with high affinity to *Ls*-AChBP. Hence, we expect this toxin to be a valuable pharmacological tool for studying the structure and function of nAChR.

AUTHOR INFORMATION

Corresponding Author

*Thomas Durek. E-mail: thomas.durek@gmail.com. Telephone: +61-7-3346-2985. Fax: +61-7-3346-2090.

Author Contributions

§C.-I.A.W. and T.R. contributed equally.

Funding

This work was supported by a National Health and Medical Research Council (NHMRC) Program Grant (569927 to P.F.A. and R.J.L.) and by The University of Queensland.

Notes

The authors declare no competing financial interest.

ACKNOWLEDGMENTS

We thank Alun Jones for help with mass spectrometry and Nikita Abraham for providing a sample of AChBP. We acknowledge use of the UQ ROCX crystallization and diffraction facility.

ABBREVIATIONS

α-EPTX-Dpp2d, α-elapitoxin-Dpp2d; nAChR, nicotinic acetylcholine receptor; TFT, three-finger toxin; BS3, bis-[sulfosuccinimidyl] suberate; MW, molecular weight; Ub−*Ls*-AChBP, ubiquitin−*Lymnia stagnalis*-acetylcholine-binding protein; rmsd, root-mean-square deviation; SEC-MALLS, size-exclusion chromatography multiangle laser light scattering

REFERENCES

(1) Utkin, Y. N. (2013) Three-finger toxins, a deadly weapon of elapid venom - Milestones of discovery. *Toxicon 62*, 50−55.

(2) Kini, R. M., and Doley, R. (2010) Structure, function and evolution of three-finger toxins: Mini proteins with multiple targets. *Toxicon 56*, 855−867.

(3) Sunagar, K., Jackson, T. N. W., Undheim, E. A. B., Ali, S. A., Antunes, A., and Fry, B. G. (2013) Three-Fingered RAVERs: Rapid Accumulation of Variations in Exposed Residues of Snake Venom Toxins. *Toxins 5*, 2172−2208.

(4) Doley, R., and Kini, R. M. (2009) Protein complexes in snake venom. *Cell. Mol. Life Sci. 66*, 2851−2871.

(5) Osipov, A. V., Kasheverov, I. E., Makarova, Y. V., Starkov, V. G., Vorontsova, O. V., Ziganshin, R. K., Andreeva, T. V., Serebryakova, M. V., Benoit, A., Hogg, R. C., Bertrand, D., Tsetlin, V. I., and Utkin, Y. N. (2008) Naturally occurring disulfide-bound dimers of three-fingered toxins - A paradigm for biological activity diversification. *J. Biol. Chem. 283*, 14571−14580.

(6) Pawlak, J., Mackessy, S. P., Sixberry, N. M., Stura, E. A., Le Du, M. H., Menez, R., Foo, C. S., Menez, A., Nirthanan, S., and Kini, R. M. (2009) Irditoxin, a novel covalently linked heterodimeric three-finger toxin with high taxon-specific neurotoxicity. *FASEB J. 23*, 534−545.

(7) Roy, A., Zhou, X. D., Chong, M. Z., D'hoedt, D., Foo, C. S., Rajagopalan, N., Nirthanan, S., Bertrand, D., Sivaraman, J., and Kini, R. M. (2010) Structural and Functional Characterization of a Novel Homodimeric Three-finger Neurotoxin from the Venom of Ophiophagus hannah (King Cobra). *J. Biol. Chem. 285*, 8302−8315.

(8) Chiappinelli, V. A., and Lee, J. C. (1985) Kappa-Bungarotoxin - Self-Association of a Neuronal Nicotinic Receptor Probe. *J. Biol. Chem. 260*, 6182−6186.

(9) Aquilina, J. A. (2009) The major toxin from the Australian Common Brown Snake is a hexamer with unusual gas-phase dissociation properties. *Proteins: Struct., Funct., Bioinf. 75*, 478−485.

(10) Battye, T. G. G., Kontogiannis, L., Johnson, O., Powell, H. R., and Leslie, A. G. W. (2011) iMOSFLM: A new graphical interface for diffraction-image processing with MOSFLM. *Acta Crystallogr. Sect. D: Biol. Crystallogr. 67*, 271−281.

(11) Storoni, L. C., McCoy, A. J., and Read, R. J. (2004) Likelihood-enhanced fast rotation functions. *Acta Crystallogr. Sect. D: Biol. Crystallogr. 60*, 432−438.

(12) Nickitenko, A. V., Michailov, A. M., Betzel, C., and Wilson, K. S. (1993) 3-Dimensional Structure of Neurotoxin-1 from Naja-Naja-Oxiana Venom at 1.9 Angstrom Resolution. *FEBS Lett. 320*, 111−117.

(13) Morris, R. J., Perrakis, A., and Lamzin, V. S. (2003) ARP/wARP and automatic interpretation of protein electron density maps. *Methods Enzymol. 374*, 229−244.

(14) Emsley, P., Lohkamp, B., Scott, W. G., and Cowtan, K. (2010) Features and development of Coot. *Acta Crystallogr. Sect. D: Biol. Crystallogr. 66*, 486−501.

(15) Vagin, A. A., Steiner, R. A., Lebedev, A. A., Potterton, L., McNicholas, S., Long, F., and Murshudov, G. N. (2004) REFMAC5 dictionary: organization of prior chemical knowledge and guidelines for its use. *Acta Crystallogr. Sect. D: Biol. Crystallogr. 60*, 2184−2195.

(16) Chen, V. B., Arendall, W. B., Headd, J. J., Keedy, D. A., Immormino, R. M., Kapral, G. J., Murray, L. W., Richardson, J. S., and Richardson, D. C. (2010) MolProbity: All-atom structure validation

for macromolecular crystallography. *Acta Crystallogr. Sect. D: Biol. Crystallogr. 66*, 12−21.
(17) Vaguine, A. A., Richelle, J., and Wodak, S. J. (1999) SFCHECK: A unified set of procedures for evaluating the quality of macromolecular structure-factor data and their agreement with the atomic model. *Acta Crystallogr. Sect. D: Biol. Crystallogr. 55*, 191−205.
(18) Potterton, E., Briggs, P., Turkenburg, M., and Dodson, E. (2003) A graphical user interface to the CCP4 program suite. *Acta Crystallogr. Sect. D: Biol. Crystallogr. 59*, 1131−1137.
(19) Bourne, Y., Talley, T. T., Hansen, S. B., Taylor, P., and Marchot, P. (2005) Crystal structure of a Cbtx-AChBP complex reveals essential interactions between snake alpha-neurotoxins and nicotinic receptors. *EMBO J. 24*, 1512−1522.
(20) De Vries, S. J., van Dijk, M., and Bonvin, A. M. J. J. (2010) The HADDOCK web server for data-driven biomolecular docking. *Nat. Protoc. 5*, 883−897.
(21) Folta-Stogniew, E., and Williams, K. R. (1999) Determination of molecular masses of proteins in solution: Implementation of an HPLC size exclusion chromatography and laser light scattering service in a core laboratory. *J. Biomol. Technol. 10*, 51−63.
(22) Debye, P. (1947) Molecular-Weight Determination by Light Scattering. *J. Phys. Colloid Chem. 51*, 18−32.
(23) Wang, C. I. A., Guncar, G., Forwood, J. K., Teh, T., Catanzariti, A. M., Lawrence, G. J., Loughlin, F. E., Mackay, J. P., Schirra, H. J., Anderson, P. A., Ellis, J. G., Dodds, P. N., and Kobe, B. (2007) Crystal structures of flax rust avirulence proteins AvrL567-A and -D reveal details of the structural basis for flax disease resistance specificity. *Plant Cell 19*, 2898−2912.
(24) Catanzariti, A. M., Soboleva, T. A., Jans, D. A., Board, P. G., and Baker, R. T. (2004) An efficient system for high-level expression and easy purification of authentic recombinant proteins. *Protein Sci. 13*, 1331−1339.
(25) Vetter, I., and Lewis, R. J. (2010) Characterization of endogenous calcium responses in neuronal cell lines. *Biochem. Pharmacol. 79*, 908−920.
(26) Fitch, R. W., Xiao, Y. X., Kellar, K. J., and Daly, J. W. (2003) Membrane potential fluorescence: A rapid and highly sensitive assay for nicotinic receptor channel function. *Proc. Natl. Acad. Sci. U. S. A. 100*, 4909−4914.
(27) Strydom, D. J. (1972) Snake venom toxins. The amino acid sequences of two toxins from Dendroaspis polylepis polylepis (black mamba) venom. *J. Biol. Chem. 247*, 4029−4042.
(28) Marcon, F., Leblanc, M., Vetter, I., Lewis, R. J., Escoubas, P., and Nicholson, G. M. (2012) Pharmacological characterization of alpha-elapitoxin-Al2a from the venom of the Australian pygmy copperhead (Austrelaps labialis): An atypical long-chain alpha-neurotoxin with only weak affinity for alpha 7 nicotinic receptors. *Biochem. Pharmacol. 84*, 851−863.
(29) Billen, B., Spurny, R., Brams, M., van Elk, R., Valera-Kummer, S., Yakel, J. L., Voets, T., Bertrand, D., Smit, A. B., and Ulens, C. (2012) Molecular actions of smoking cessation drugs at alpha 4 beta 2 nicotinic receptors defined in crystal structures of a homologous binding protein. *Proc. Natl. Acad. Sci. U. S. A. 109*, 9173−9178.
(30) Dewan, J. C., Grant, G. A., and Sacchettini, J. C. (1994) Crystal-Structure of Kappa-Bungarotoxin at 2.3-Angstrom Resolution. *Biochemistry 33*, 13147−13154.
(31) Nirthanan, S., and Gwee, M. C. E. (2004) Three-finger alpha-neurotoxins and the nicotinic acetylcholine receptor, forty years on. *J. Pharmacol. Sci. 94*, 1−17.
(32) Grant, G. A., and Chiappinelli, V. A. (1985) κ-Bungarotoxin: Complete Amino-Acid Sequence of a Neuronal Nicotinic Receptor Probe. *Biochemistry 24*, 1532−1537.
(33) Hofmann, K., and Bergmann, M. (1941) The kinetics of the action of trypsin upon synthetic substrates. *J. Biol. Chem. 138*, 243−248.
(34) Merkler, D. J. (1994) C-Terminal Amidated Peptides - Production by the in-Vitro Enzymatic Amidation of Glycine-Extended Peptides and the Importance of the Amide to Bioactivity. *Enzyme Microb. Technol. 16*, 450−456.
(35) Maeda, N., and Tamiya, N. (1978) 3 Neurotoxins from Venom of a Sea Snake Astrotia-Stokesii, Including 2 Long-Chain Neurotoxic Proteins with Amidated C-Termini. *Biochem. J. 175*, 507−517.
(36) Correa-Netto, C., Junqueira-de-Azevedo, I. D. M., Silva, D. A., Ho, P. L., Leitao-de-Araujo, M., Alves, M. L. M., Sanz, L., Foguel, D., Zingali, R. B., and Calvete, J. J. (2011) Snake venomics and venom gland transcriptomic analysis of Brazilian coral snakes, Micrurus altirostris and M. corallinus. *J. Proteomics 74*, 1795−1809.
(37) Chatrath, S. T., Chapeaurouge, A., Lin, Q. S., Lim, T. K., Dunstan, N., Mirtschin, P., Kumar, P. P., and Kini, R. M. (2011) Identification of Novel Proteins from the Venom of a Cryptic Snake *Drysdalia coronoides* by a Combined Transcriptomics and Proteomics Approach. *J. Proteome Res. 10*, 739−750.
(38) Fruchart-Gaillard, C., Gilquin, B., Antil-Delbeke, S., Le Novere, N., Tamiya, T., Corringer, P. J., Changeux, J. P., Menez, A., and Servent, D. (2002) Experimentally based model of a complex between a snake toxin and the alpha 7 nicotinic receptor. *Proc. Natl. Acad. Sci. U. S. A. 99*, 3216−3221.
(39) Rosenthal, J. A., Levandoski, M. M., Chang, B., Potts, J. F., Shi, Q. L., and Hawrot, E. (1999) The functional role of positively charged amino acid side chains in α-bungarotoxin revealed by site-directed mutagenesis of a His-tagged recombinant α-bungarotoxin. *Biochemistry 38*, 7847−7855.
(40) Endo, T., Oya, M., Tamiya, N., and Hayashi, K. (1987) Role of C-Terminal Tail of Long Neurotoxins from Snake-Venoms in Molecular-Conformation and Acetylcholine-Receptor Binding - Proton Nuclear-Magnetic-Resonance and Competition Binding-Studies. *Biochemistry 26*, 4592−4598.
(41) Dutertre, S., Ulens, C., Buttner, R., Fish, A., van Elk, R., Kendel, Y., Hopping, G., Alewood, P. F., Schroeder, C., Nicke, A., Smit, A. B., Sixma, T. K., and Lewis, R. J. (2007) AChBP-targeted alpha-conotoxin correlates distinct binding orientations with nAChR subtype selectivity. *EMBO J. 26*, 3858−3867.
(42) Maslennikov, I. V., Shenkarev, Z. O., Zhmak, M. N., Ivanov, V. T., Methfessel, C., Tsetlin, V. I., and Arseniev, A. S. (1999) NMR spatial structure of alpha-conotoxin ImI reveals a common scaffold in snail and snake toxins recognizing neuronal nicotinic acetylcholine receptors. *FEBS Lett. 444*, 275−280.
(43) Osipov, A. V., Astapova, M. V., Tsetlin, V. I., and Utkin, Y. N. (2004) The first representative of glycosylated three-fingered toxins - Cytotoxin from the Naja kaouthia cobra venom. *Eur. J. Biochem. 271*, 2018−2027.

NOTE ADDED AFTER ASAP PUBLICATION

This paper was published ASAP on June 5, 2014. Figure 2 has been updated and the corrected version was reposted on June 6, 2014.